

# Selective Synthesis of Ruthenium(II) Metalla[2]Catenane via Solvent and Guest-Dependent Self-Assembly

HyeWoo Lee,<sup>†,||</sup> Palani Elumalai,<sup>†,||</sup> Nem Singh,<sup>†</sup> Hyunuk Kim,<sup>‡</sup> Sang Uck Lee,<sup>§</sup> and Ki-Wan Chi<sup>\*,†</sup>

<sup>†</sup>Department of Chemistry, University of Ulsan, Ulsan 680-749, Republic of Korea

<sup>‡</sup>Energy Materials Lab, Korea Institute of Energy Research, Daejeon 305-343, Republic of Korea

<sup>§</sup>Department of Applied Chemistry, Hanyang University, Ansan 426-791, Republic of Korea

## Supporting Information

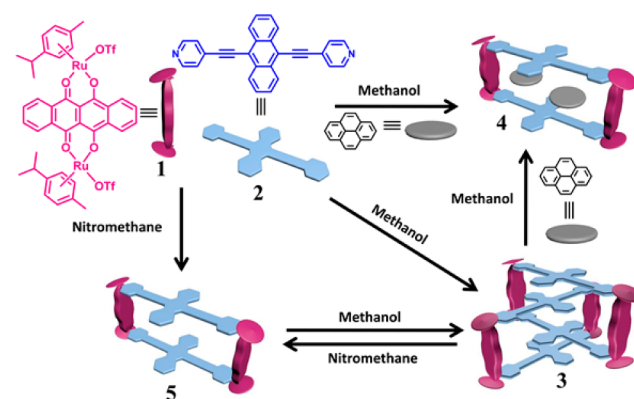
**ABSTRACT:** The coordination-driven self-assembly of an anthracene-functionalized ditopic pyridyl donor and a tetracene-based dinuclear Ru(II) acceptor resulted in an interlocked metalla[2]catenane,  $[M_2L_2]_2$ , in methanol and a corresponding monorectangle,  $[M_2L_2]$ , in nitromethane. Subsequently, guest template, solvent, and concentration effects allowed the self-assembly to be reversibly fine-tuned among monorectangle and catenane structures.

Over the past few decades, significant progress has been made in the construction of new classes of two and three-dimensional (2D and 3D) supramolecular coordination-driven self-assemblies.<sup>1–3</sup> Interest in interlocked molecular architectures is rapidly growing not only because of their intriguing structures<sup>4</sup> and topological importance<sup>5</sup> but also because of their potential applications in various fields including catalysis, host–guest chemistry, energy harvesting, and biomedical applications.<sup>6,7</sup> Beyond their aesthetic appeal, interlocked molecular links are worthy synthetic targets that expand a chemist’s repertoire of potential building blocks for engineering and smart materials.<sup>8</sup> The recent improvements in synthetic paradigms have allowed the preparation of diverse catenanes and more complex structures such as trefoil knots,<sup>9</sup> Solomon links,<sup>10</sup> and Borromean rings<sup>5a,11</sup> in high yields. Discrete self-assembled molecular species consisting of interlinked chainlike molecules are of great interest because of their fascinating structures and potential applications for drug delivery systems, molecular capsules, and nanoscale devices.<sup>12</sup> One fascinating and challenging synthetic target comprising entangled bodies is molecular metallacatenane.<sup>13</sup> The formation of interlocked metallomacrocycles oftentimes involves molecular recognition and/or host–guest chemistry based on non-covalent van der Waals forces, thereby facilitating the preorganization of molecular components and significantly improving synthetic efficiency.<sup>14</sup>

We recently reported a self-assembled arene–Ru-based noncatenane metallarectangle that encapsulated a second identical rectangle in a “molecule-in-molecule” motif, likely through  $\pi$ – $\pi$  and other non-covalent interactions.<sup>15</sup> Herein we report a supramolecular self-assembled metalla[2]catenane in which two identical rectangles are interlocked by multiple strong  $\pi$ – $\pi$  interactions, as evidenced by single-crystal X-ray diffraction (scXRD). The organometallic arene–Ru-based interlocked metalla[2]catenane and molecular rectangle were achieved

from the arene–Ru(II) acceptor **1** and the  $\pi$ -bond-rich rigid ditopic anthracene-based pyridyl-functionalized N-donor ligand 9,10-bis(pyridin-4-ylethynyl)anthracene (**2**) (Scheme 1). Treat-

**Scheme 1. Schematic Representation of the Formation of Metalla[2]catenane **3**, Pyrene-Encapsulating Rectangle **4**, and Monorectangle **5****

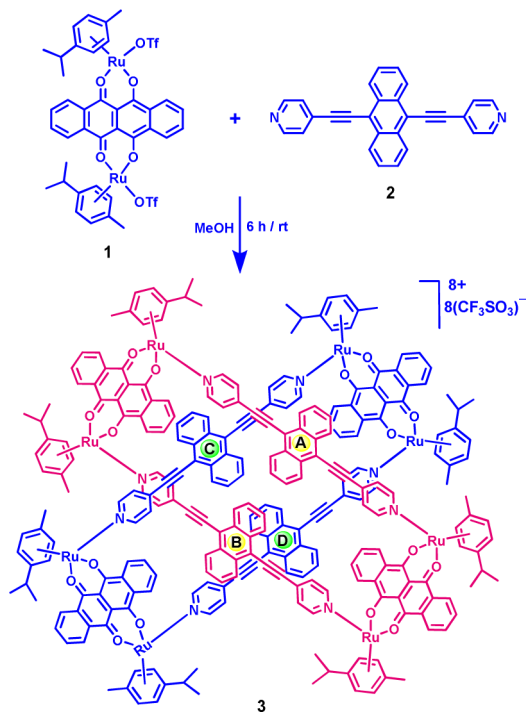


ing **1** with an equimolar amount of **2** in methanol-*d*<sub>4</sub> afforded metalla[2]catenane **3** (Scheme 2). The <sup>1</sup>H NMR spectrum of the isolated product interestingly showed that all of the sets of proton resonances were doubled into two signals. Two sets of signals for the  $\alpha$ -pyridinyl protons were observed at 8.65 and 8.54 ppm. Similarly, two sets of doublets were observed corresponding to the  $\beta$ -pyridinyl protons at 7.25 and 7.01 ppm. In the same way, the anthracene protons were observed as four doublets of doublets at 7.66, 7.11, 6.33, and 5.04 ppm. The large upfield shift of the anthracene proton resonances is due to the increased shielding by the  $\pi$ -electron-rich nature of the adjacent triple-bond moieties. The tetracene protons were observed as four multiplets at 8.93 ppm (two multiplets overlapped for H<sub>5</sub>, 16H) and 8.11 ppm (two multiplets overlapped for H<sub>6</sub>, 16H) with a noticeable downfield shift compared with the <sup>1</sup>H NMR spectrum of **1**. The aryl protons of the *p*-cymene moieties of **3** were observed as four doublets at 6.17, 6.06, 5.92, and 5.79 ppm. All of the <sup>1</sup>H NMR peak assignments were supported by <sup>1</sup>H–<sup>1</sup>H rotating-frame nuclear Overhauser effect spectroscopy (ROESY) and <sup>13</sup>C NMR data (see Figures S1–S3 in the Supporting

Received: March 11, 2015

Published: March 30, 2015

## Scheme 2. One-Pot Synthesis of Interlocked Metalla[2]catenane 3



Information (SI)). The ESI-MS spectrum of interlocked **3** confirmed the  $[M_2L_2]_2$  composition with a prominent signal at  $m/z$  1767.75 ( $[M - 3OTf]^{3+}$ ; Figure 1). The experimentally observed and theoretically calculated isotopic distributions were in excellent agreement.

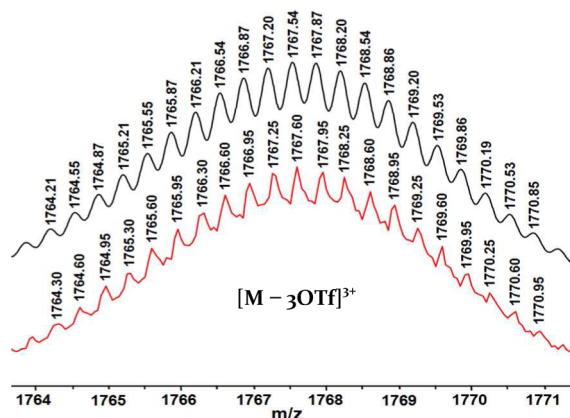


**Figure 1.** Calculated (black, top) and experimental (red, bottom) ESI-MS spectra of **3**.

The structure of the interlocked metalla[2]catenane **3** was unambiguously confirmed by scXRD analysis using synchrotron radiation. A single crystal suitable for XRD analysis was obtained by slow vapor diffusion of diethyl ether into a methanol solution of **3** at room temperature. The interlocked dimeric nature of **3** was confirmed upon structural refinement, which clearly revealed the interlocked metalla[2]catenane (Figure 2). A noteworthy feature of the catenane structure is that the two rectangles are interlocked in a quadruple fashion. The interlocked metalla[2]catenane **3** is stabilized by several strong  $\pi$ - $\pi$  stacking interactions between anthracene moieties of **2** and naphthacene-

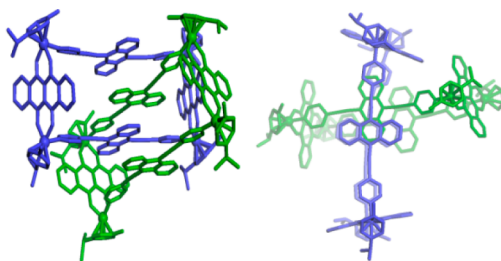


**Figure 2.** Crystal structure of **3**: (left) side view; (right) top view. H atoms, counterions, and solvents of crystallization have been omitted for clarity.

nedione moieties of **1**. Strong sandwich-type  $\pi$ - $\pi$  stacking between the anthracene moieties of the ligand was observed, with A-C, C-B, and B-D distances of 3.657, 3.618, and 3.571 Å, respectively (where A, B, C, and D denote the ligand anthracene moieties, as shown in Scheme 2). Interestingly, one of the corner phenyl rings of the anthracene moiety and a corner phenyl ring of the naphthacenedione moiety are stabilized by bifurcated edge-to-face-type T-shaped C-H $\cdots$  $\pi$  interactions, with C104-C211,173 and C4,7-C118 distances of 3.378 and 3.649 Å, respectively. Notably, there are several strong intermolecular  $\pi$ - $\pi$ , C-H $\cdots$  $\pi$ , C-H $\cdots$ O, and C-H $\cdots$ F interactions between the interlocked moiety with triflate counterions and solvent molecules present in the crystal lattice (Figure S4).

To understand the importance of  $\pi$ - $\pi$  interactions and the role of other non-covalent interactions on the formation of the interlocked metalla[2]catenane **3**, experiments were performed in the presence of  $\pi$ -bond-rich pyrene guest molecules to inhibit the intermolecular  $\pi$ - $\pi$  interactions between the rectangles.<sup>16</sup> Upon gradual addition of an excess amount of pyrene to a methanol- $d_4$  solution of **3** for a period of 5 min, the resulting reaction mixture was stirred for 2 h at 40 °C. The  $^1\text{H}$  NMR spectral patterns of the solution changed because of the formation of  $M_2L_2(\text{pyrene})_2$ . The simpler  $^1\text{H}$  NMR spectrum obtained clearly supports the formation of **4**. Two doublets at 8.32 and 6.62 ppm for the pyridinyl  $\alpha$  and  $\beta$  protons, respectively, were observed in the  $^1\text{H}$  NMR spectrum of the reaction mixture. The anthracene protons were observed as two multiplets at 7.53 and 7.35 ppm. The *p*-cymene aryl protons were observed at 6.00 and 5.70 ppm, and the tetracene protons were observed as two multiplets at 8.96 and 8.20 ppm. The peaks associated with the pyrene were shifted in the spectrum of **4** versus free pyrene (Figures S5 and S6).

To confirm the encapsulation of the pyrene guest, scXRD analysis was performed for the resulting crystals of **4**. A single crystal of **4** suitable for XRD analysis was obtained by slow evaporation of methanol solution over several days at room temperature. The structural analysis unambiguously confirmed the rectangular nature of **4** (Figure 3), in which two pyrene molecules are encapsulated inside the cavity in a parallel fashion, with each ethynyl-pyridinyl-ethynyl moiety stabilized via  $\pi$ - $\pi$  interactions (3.338 and 3.380 Å). Interestingly, T-shaped  $\pi$ - $\pi$  stacking was observed between a pyrene ring and one naphthacenedione acceptor moiety. The  $\pi$ - $\pi$  stacking distance between the centroid of the second ring of the naphthacenedione and one of the pyrene rings is 3.412 Å. Notably, the two parallel anthracene moieties of the ligand are closer to each other in rectangle **4** because of these strong  $\pi$ - $\pi$  interactions. The distance between the upper and lower anthracene rims is 6.419 Å, which is almost 2 Å shorter than the Ru1-Ru2 distance in the

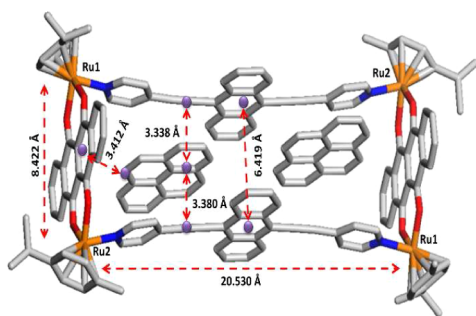


**Figure 3.** X-ray crystal structure of **4**. H atoms, counterions, and solvents of crystallization have been omitted for clarity.

acceptor (8.422 Å). The length of the rectangle is 20.530 Å. The  $^1\text{H}$  NMR spectrum and crystal structure results indicate that the formation of **3** was disrupted by the  $\pi$ - $\pi$  interactions between the pyrenes and metallarectangles. A similar reaction was performed directly by adding excess pyrene to the  $\text{CD}_3\text{OD}$  solution of arene-Ru acceptor and an equimolar amount of N-donor solution with 24 h of stirring. The  $^1\text{H}$  NMR spectral patterns of the resulting complexes matched those of the previously prepared **4** (Scheme 1).

Interestingly the identical reaction of arene-Ru acceptor **1** and N-donor **2** in nitromethane- $d_3$  afforded the tetranuclear monorectangle [ $\text{M}_2\text{L}_2$ ] **5**, in contrast to the metalla[2]catenane obtained in methanol. The simple  $^1\text{H}$  NMR spectral pattern provided the clue for the formation of **5**. Two doublets at 8.60 and 7.49 ppm for the pyridinyl protons were observed in the  $^1\text{H}$  NMR spectrum of the reaction mixture. The anthracene protons were observed as two doublets of doublets at 8.08 and 7.30 ppm. The *p*-cymene aryl protons were observed at 6.01 and 5.77 ppm, and the tetracene protons were observed as two doublets of doublets at 8.83 and 8.02 ppm. The peaks associated with acceptor **1** were shifted in the spectrum of **5** versus that of free **1** (Figure S7). For further understanding of the solvent effect, metalla[2]catenane **3** was dissolved in the polar aprotic solvent nitromethane- $d_3$ , and the solution was stirred for 2 h at 50 °C (Scheme 1). The  $^1\text{H}$  NMR spectrum of the resulting compound matched that of monorectangle **5**, indicating that the mono versus catenane nature of the self-assembled architecture depends on the solvent used. The concentration also plays a key role in the selective self-assembly. When the concentration of monorectangle **5** was  $\leq 2$  mM in nitromethane- $d_3$ , no changes were found, whereas when the concentration of **5** increased to  $>2$  mM, the formation of **3** was observed in minor amounts, as verified by  $^1\text{H}$  NMR analysis (Figure S8). The ESI-MS spectra of **4** and **5** also matched, except that **4** showed an additional peak at 203.90  $[\text{M} + \text{H}]^+$  for pyrene (Figures S10 and S11). The isotopic distributions of **4** and **5** for prominent peaks at 1289.41  $[\text{M} - 2(\text{pyrene}) - 2\text{OTf}]^{2+}$  and 1289.23  $[\text{M} - 2\text{OTf}]^{2+}$ , respectively, were also identical (Figure S12).

Diffusion-ordered spectroscopy (DOSY) and  $^1\text{H}$ - $^1\text{H}$  ROESY NMR analysis were performed to confirm the structures in solution.<sup>17</sup> The ROESY spectra of **3** and **5** (Figures S2 and S13) are in good agreement with the associated  $^1\text{H}$  NMR spectra. In the spectrum of **5**, only one coupling interaction was observed between the  $\alpha,\beta$ -anthracenyl protons of ligand **2**, whereas multiple couplings were observed for the  $\alpha,\beta$ -anthracenyl moiety of **3** because of the interlocked structure. The 2D DOSY NMR spectra of both interlocked metalla[2]catenane **3** and pyrene-encapsulating rectangle **4** were recorded separately in methanol-

$d_4$  at 298 K (Figures S14 and S15) and revealed diffusion coefficients ( $D$ ) of  $4.4 \times 10^{-10}$  and  $5.4 \times 10^{-10} \text{ m}^2 \text{ s}^{-1}$ , respectively. The DOSY NMR analysis of the products formed in nitromethane further confirmed the concentration effect. At a low concentration of **5** (0.78 mM),  $D = 5.4 \times 10^{-10} \text{ m}^2 \text{ s}^{-1}$  was obtained, whereas at high concentration (2.10 mM), a set of DOSY patterns with two different diffusion coefficients,  $D = 4.4 \times 10^{-10}$  and  $5.4 \times 10^{-10} \text{ m}^2 \text{ s}^{-1}$  were observed. The lower  $D$  value matches well with the diffusion coefficient of **3**, and the other  $D$  value matches that of **4** ( $5.4 \times 10^{-10} \text{ m}^2 \text{ s}^{-1}$ ) (Figure 4 and S14–

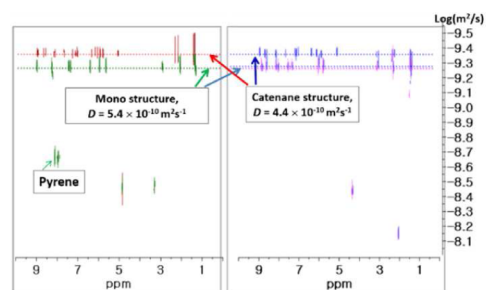


**Figure 4.** DOSY NMR spectra of (a) **3** (red) and **4** (green) in  $\text{CD}_3\text{OD}$  and (b) **5** (pink) and the mixture of **3** and **5** (blue) in  $\text{CD}_3\text{NO}_2$ .

S17). The DOSY, ROESY, ESI-MS, and scXRD data prove that self-assembled architectures **4** and **5** have the same skeleton (Figure S18). The UV-vis and emission spectra of **3** and **5** along with those of acceptor **1** and donor **2** were investigated, and these data also support the structure of **5** (see the SI).

Density functional theory (DFT) binding energy calculations were performed at the PBE/DNP level<sup>18a</sup> with the conductor-like screening model (COSMO)<sup>18b,c</sup> method for newly synthesized interlocked metalla[2]catenane **3**, pyrene-encapsulating metallacapsule **4**, and monorectangle **5** to investigate the stability of the self-assemblies in methanol. The calculated binding energy of **3** was 1.89 kcal/mol, which is 31 times weaker than that of **4** (59.61 kcal/mol); the calculated energies of **3** and **5** are within error. These theoretical calculations clearly indicate that higher energy is required to disassemble the pyrene encapsulated metallacapsule **4** than the interlocked metalla[2]catenane **3** and metallarectangle **5**. Previously, Mukherjee and co-workers also observed triply interlocked  $\text{Pd}_{12}$  coordination prisms that were converted into non-interlocked  $\text{Pd}_6$  prisms through  $\pi$ - $\pi$  stacking interactions upon the addition of an aromatic guest.<sup>17b</sup> These experimental results, theoretical calculations, and previous literature reports support that strong  $\pi$ - $\pi$  interactions make pyrene-encapsulating **4** more stable than **3** and **5** (Tables S1 and S2 in the SI).

In conclusion, treating a tetracene-based arene-Ru(II) acceptor with an anthracene-based donor in methanol affords an interlocked metalla[2]catenane, whereas the same reaction carried out with pyrene as a guest results in a pyrene-encapsulating mono-metallarectangle in which two guest molecules are bound in the aromatic cavity through host-guest interactions. The strength of the guest interaction can also be used to disassemble the metalla[2]catenane with high fidelity. Interestingly, a similar reaction done in nitromethane, even without pyrene, affords a monorectangle instead of the catenane. DFT calculations, 2D ROESY and DOSY data in solution, and solid-state structures show that the formation of the interlocked metalla[2]catenane is preferred to the non-interlocked metallarectangle in the polar protic solvent methanol. In nitromethane,

the low concentration reaction selectively produces the non-interlocked metallarectangle, whereas a mixture of catenane and monostructure is formed at high concentration. This new synthetic strategy would be promising for the selective self-assembly of catenane and noncatenane molecular architectures.

## ■ ASSOCIATED CONTENT

### ■ Supporting Information

Experimental details, elemental analysis data,  $^1\text{H}$  and  $^{13}\text{C}$  NMR spectra of 3–5, 2D  $^1\text{H}$ – $^1\text{H}$  ROESY and DOSY NMR data, and CIF files for 3 and 4 (CCDC 1031287–1031288). This material is available free of charge via the Internet at <http://pubs.acs.org>.

## ■ AUTHOR INFORMATION

### Corresponding Author

\*kwchi@ulsan.ac.kr.

### Author Contributions

<sup>||</sup>H.L. and P.E. contributed equally.

### Notes

The authors declare no competing financial interest.

## ■ ACKNOWLEDGMENTS

This study was supported by the Basic Science Research Program through the National Research Foundation of Korea (NRF) funded by the Ministry of Science, ICT, and Future Planning (NRF-2013R1A1A2006859) and the Ministry of Education (NRF-2014R1A1A2007828 and NRF-2014R1A1A2007897). Support from the Priority Research Centers Program (2009-0093818) through the NRF is also appreciated. H.K. also thanks to Research and Development Project of KIER (B5-2513). XRD experiments using synchrotron radiation were performed at the Pohang Accelerator Laboratory in Korea.

## ■ REFERENCES

- (1) (a) Stang, P. J.; Olenyuk, B. *Acc. Chem. Res.* **1997**, *30*, 502. (b) Leininger, S.; Olenyuk, B.; Stang, P. J. *Chem. Rev.* **2000**, *100*, 853. (c) Swiegers, G. F.; Malefetse, T. J. *Chem. Rev.* **2000**, *100*, 3483. (d) Holliday, B. J.; Mirkin, C. A. *Angew. Chem., Int. Ed.* **2001**, *40*, 2022. (e) Seidel, S. R.; Stang, P. J. *Acc. Chem. Res.* **2002**, *35*, 972. (f) Fujita, M.; Tominaga, M.; Hori, A.; Therrien, B. *Acc. Chem. Res.* **2005**, *38*, 369. (g) Northrop, B. H.; Zheng, Y.-R.; Chi, K.-W.; Stang, P. J. *Acc. Chem. Res.* **2009**, *42*, 1554. (h) Murase, T.; Otsuka, K.; Fujita, M. *J. Am. Chem. Soc.* **2010**, *132*, 7864.
- (2) (a) Chakrabarty, R.; Mukherjee, P. S.; Stang, P. J. *Chem. Rev.* **2011**, *111*, 6810. (b) Schmitt, F.; Freudenreich, J.; Barry, N. P. E.; Juillerat-Jeanneret, L.; Süß-Fink, G.; Therrien, B. *J. Am. Chem. Soc.* **2012**, *134*, 754. (c) Freye, S.; Hey, J.; Torras-Galán, A.; Stalke, D.; Herbst-Irmer, R.; John, M.; Clever, G. H. *Angew. Chem., Int. Ed.* **2012**, *51*, 2191. (d) Xie, T.-Z.; Guo, C.; Yu, S. Y.; Pan, Y. J. *Angew. Chem., Int. Ed.* **2012**, *51*, 1177. (e) Cook, T. R.; Vajpayee, V.; Lee, M. H.; Stang, P. J.; Chi, K.-W. *Acc. Chem. Res.* **2013**, *46*, 2464. (f) Shanmugaraju, S.; Vajpayee, V.; Lee, S.; Chi, K.-W.; Mukherjee, P. S. *Inorg. Chem.* **2012**, *51*, 4817. (g) Shanmugaraju, S.; Jadhav, H.; Patil, Y. P.; Mukherjee, P. S. *Inorg. Chem.* **2012**, *51*, 13072. (h) Cook, T. R.; Zheng, Y.-R.; Stang, P. J. *Chem. Rev.* **2013**, *113*, 734.
- (3) (a) Zhang, W.-Y.; Han, Y.-F.; Weng, L.-H.; Jin, G.-X. *Organometallics* **2014**, *33*, 3091. (b) Li, H.; Han, Y.-F.; Lin, Y.-J.; Guo, Z.-W.; Jin, G.-X. *J. Am. Chem. Soc.* **2014**, *136*, 2982. (c) Jin, Y.; Wang, Q.; Taynton, P.; Zhang, W. *Acc. Chem. Res.* **2014**, *47*, 1575. (d) Li, K.; Zhang, L. Y.; Yan, C.; Wei, S. C.; Pan, M.; Zhang, L.; Su, C. Y. *J. Am. Chem. Soc.* **2014**, *136*, 4456.
- (4) (a) Mukherjee, S.; Mukherjee, P. S. *Chem. Commun.* **2014**, *50*, 2239 and references therein. (b) Amabilino, D. B.; Stoddart, J. F. *Chem. Rev.* **1995**, *95*, 2725. (c) Beves, J. E.; Blight, B. A.; Campbell, C. J.; Leigh, D.

A.; McBurney, R. T. *Angew. Chem., Int. Ed.* **2011**, *50*, 9260. (d) Fujita, M. *Acc. Chem. Res.* **1999**, *32*, 53.

(5) (a) Forgan, R. S.; Sauvage, J.-P.; Stoddart, J. F. *Chem. Rev.* **2011**, *111*, 5434. (b) Durot, S.; Taesch, J.; Heitz, V. *Chem. Rev.* **2014**, *114*, 8542.

(6) Prakasam, T.; Lusi, M.; Elhabiri, M.; Platas-Iglesias, C.; Olsen, J.-C.; Asfari, Z.; Cianferani-Sanglier, S.; Debaene, F.; Charbonniere, L. J.; Trabolsi, A. *Angew. Chem., Int. Ed.* **2013**, *52*, 9956 and references therein.

(7) (a) Dietrich-Buchecker, C.; Rapenne, G.; Sauvage, J.-P. *Molecular Catenanes, Rotaxanes and Knots*; Wiley-VCH: Weinheim, Germany, 2007; p 107. (b) Huang, S.-L.; Lin, Y.-J.; Hor, T. S. A.; Jin, G.-X. *J. Am. Chem. Soc.* **2013**, *135*, 8125 and references therein.

(8) (a) Ayme, J.-F.; Beves, J. E.; Campbell, C. J.; Leigh, D. A. *Chem. Soc. Rev.* **2013**, *42*, 1700. (b) Fenlon, E. E. *Eur. J. Org. Chem.* **2008**, 5023. (c) Lukin, O.; Vögtle, F. *Angew. Chem., Int. Ed.* **2005**, *44*, 1456. (d) Stoddart, J. F. *Chem. Soc. Rev.* **2009**, *38*, 1802.

(9) (a) Ayme, J.-F.; Beves, J. E.; Leigh, D. A.; McBurney, R. T.; Rissanen, K.; Schultz, D. J. *J. Am. Chem. Soc.* **2012**, *134*, 9488. (b) Ayme, J.-F.; Gil-Ramirez, G.; Leigh, D. A.; Lemonnier, J.-F.; Markevicius, A.; Murnyn, C. A.; Zhang, G. J. *J. Am. Chem. Soc.* **2014**, *136*, 13142. (c) Meyer, M.; Albrecht-Gary, A.-M.; Dietrich-Buchecker, C. O.; Sauvage, J.-P. *J. Am. Chem. Soc.* **1997**, *119*, 4599.

(10) (a) Nierengarten, J. F.; Dietrich-Buchecker, C. O.; Sauvage, J. P. *J. Am. Chem. Soc.* **1994**, *116*, 375. (b) Peinador, C.; Blanco, V.; Quintela, J. M. *J. Am. Chem. Soc.* **2009**, *131*, 920. (c) Pentecost, C. D.; Chichak, K. S.; Peters, A. J.; Cave, G. W. V.; Cantrill, S. J.; Stoddart, J. F. *Angew. Chem., Int. Ed.* **2007**, *46*, 218. (d) McArdle, C. P.; Vittal, J. J.; Puddephatt, R. J. *Angew. Chem., Int. Ed.* **2000**, *39*, 3819. (e) McArdle, C. P.; Jennings, M. C.; Vittal, J. J.; Puddephatt, R. J. *Chem.—Eur. J.* **2001**, *7*, 3572.

(11) (a) Chichak, K. S.; Cantrill, S. J.; Pease, A. R.; Chiu, S.-H.; Cave, G. W. V.; Atwood, J. L.; Stoddart, J. F. *Science* **2004**, *304*, 1308. (b) Huang, S.-L.; Lin, Y.-L.; Li, Z.-H.; Jin, G.-X. *Angew. Chem., Int. Ed.* **2014**, *53*, 11218 and references therein.

(12) (a) Schalley, C. A.; Lützen, A.; Albrecht, M. *Chem.—Eur. J.* **2004**, *10*, 1072. (b) Mishra, A.; Kang, S. C.; Chi, K.-W. *Eur. J. Inorg. Chem.* **2013**, 5222. (c) Leigh, D. A.; Wong, J. K. Y.; Dehez, F.; Zerbetto, F. *Nature* **2003**, *424*, 174. (d) Therrien, B.; Süß-Fink, G.; Govindaswamy, P.; Renfrew, A. K.; Dyson, P. J. *Angew. Chem., Int. Ed.* **2008**, *47*, 3773.

(13) (a) Yamashita, K.; Kawano, M.; Fujita, M. *J. Am. Chem. Soc.* **2007**, *129*, 1850. (b) Fujita, M.; Fujita, N.; Ogura, K.; Yamaguchi, K. *Nature* **1999**, *400*, 52. (c) Li, S.; Huang, J.; Cook, T. R.; Pollock, J. B.; Kim, H.; Chi, K. W.; Stang, P. J. *J. Am. Chem. Soc.* **2013**, *135*, 2084. (d) Fujita, M.; Ibukuro, F.; Hagihara, H.; Ogura, K. *Nature* **1994**, *367*, 720.

(14) (a) Mishra, A.; Dubey, A.; Min, J. W.; Kim, H.; Stang, P. J.; Chi, K.-W. *Chem. Commun.* **2014**, *50*, 7542. (b) Harris, K.; Sun, Q.-F.; Sato, S.; Fujita, M. *J. Am. Chem. Soc.* **2013**, *135*, 12497. (c) Fang, Y.; Murase, T.; Sato, S.; Fujita, M. *J. Am. Chem. Soc.* **2013**, *135*, 613.

(15) Vajpayee, V.; Song, Y. H.; Cook, T. R.; Kim, H.; Lee, Y.; Stang, P. J.; Chi, K.-W. *J. Am. Chem. Soc.* **2011**, *133*, 19646.

(16) (a) Freudenreich, J.; Furrer, J.; Süß-Fink, S.; Therrien, B. *Organometallics* **2011**, *30*, 942. (b) Barry, N. P. E.; Furrer, J.; Freudenreich, J.; Süß-Fink, G.; Therrien, B. *Eur. J. Inorg. Chem.* **2010**, 725.

(17) (a) Freudenreich, J.; Dalvit, C.; Süß-Fink, G.; Therrien, B. *Organometallics* **2013**, *32*, 3018. (b) Bar, A. K.; Raghobhama, S.; Moon, D.; Mukherjee, P. S. *Chem.—Eur. J.* **2012**, *18*, 3199.

(18) (a) Perdew, J. P.; Burke, K.; Ernzerhof, M. *Phys. Rev. Lett.* **1996**, *77*, 3865. (b) Klamt, A.; Schüürmann, G. *J. Chem. Soc., Perkin Trans. 2* **1993**, 799. (c) Delley, B. *Mol. Simul.* **2006**, *32*, 117.